

# Efficient superoscillation measurement for incoherent optical imaging

Mankei Tsang

**Abstract**—I propose a superoscillation measurement method for subdiffraction incoherent optical sources, with potential applications in astronomy, remote sensing, fluorescence microscopy, and spectroscopy. The proposal, based on coherent optical processing, can capture all the light on the aperture in principle, perform better than direct imaging on statistical terms, and approach the fundamental quantum limit.

## I. INTRODUCTION

Improving the resolution of an optical imaging system beyond the diffraction limit has been a dream of opticians and a subject of intense research for centuries [1]. Superresolution research has two elephants in the room, however: signal-to-noise ratio (SNR) and competition with computational techniques, such as deconvolution [1]. Research on superoscillation, which has received renewed interest in recent years [2], is no exception. Existing techniques rely on masking parts of the aperture, meaning that a significant portion of the light is lost. It is also unclear whether the enhancement is superior to that obtainable by digital image processing together with full-aperture direct imaging, which can capture as much light as the aperture allows.

Building on the recent work on quantum-inspired superresolution [3], [4], here I show how a superoscillation measurement can be implemented for incoherent sources without losing any of the light in principle. I also show that the resultant error is much lower than that obtainable by direct imaging with image processing for subdiffraction objects. In fact, the error is close to the quantum limit according to the quantum Cramér-Rao bound (QCRB) [5], so there is little room for further improvement, as far as passive imaging is concerned. The proposed method works in the far field, requires only known optical technologies and materials, and has diverse potential applications in astronomy, remote sensing, fluorescence microscopy, and spectroscopy.

The key insight of this work is that the Fourier coefficients of an object intensity function, in terms of a basis of superoscillatory functions, can be constructed from the object moments. As the moments can be measured efficiently via spatial-mode demultiplexing (SPADE) [6], [7], [8], [9], [10], [11], [12], [13], [14], the Fourier coefficients can also be measured efficiently. This work hence serves as a bridge

between the traditional treatment of superresolution based on Fourier analysis and the nascent field of quantum-inspired incoherent imaging, which has so far focused on special parametric models or moment estimation only.

The theory here turns out to share some similarities with the singular-system approach pioneered by Slepian and Bertero [1], [15], [16] as well. This connection is not surprising, considering that the singular-system approach is intimately related to superoscillation [1], but it is still satisfying to have a unified picture here. The important difference of the proposal here from the method proposed by Bertero and coworkers for incoherent imaging [16], [17] is that the former involves coherent optical processing, whereas the latter processes the image-plane intensity only and is subject to the same limits as those for direct imaging.

The statistical and quantum analysis here is novel in the context of superoscillation research [2]. It is noteworthy that Kolobov and coworkers performed a similar kind of analysis for coherent imaging in the context of the singular-system approach [18], [19], [20], [21], but they did not study the incoherent case, which is arguably more important in optics. Besides the obvious necessity of considering incoherent sources for astronomy and remote sensing, it is also necessary to use incoherent fluorophores in biological microscopy to provide protein-specific tagging and contrast [22], [23], [24], [25]; label-free optical methods are unable to provide such contrast and also cannot compete with electron microscopy in many applications. Compared with existing superresolution techniques in fluorescence microscopy that manipulates the fluorophore emission [23], [24], [25], far-field methods that extract more information from the light may complement or supersede them by covering for their shortcomings, such as slow speed and phototoxicity.

To be sure, the achievable resolution enhancement is still severely limited by the photon budget and the object size. It is in the sense of making almost the best use of the incoming photons that I claim the measurement to be efficient.

## II. REVIEW OF SUPERRESOLUTION AND SUPEROSCILLATION

To set the stage, I first review the concepts of superresolution and superoscillation that are relevant to this work. This section is mostly based on Ref. [1].

Let  $\mathcal{F}$  be the input function space, where each element is a function  $F : D \rightarrow E$  that determines the optical fields emitted by an object on the object plane. Define similarly an output function space  $\mathcal{F}'$ , which consists of output signals

This research is supported by the National Research Foundation (NRF) Singapore, under its Quantum Engineering Programme (Award QEP-P7). Mankei Tsang is with the Department of Electrical and Computer Engineering, National University of Singapore, 4 Engineering Drive 3, Singapore 117583 and the Department of Physics, National University of Singapore, 2 Science Drive 3, Singapore 117551 (email: [mankei@nus.edu.sg](mailto:mankei@nus.edu.sg), website: <https://blog.nus.edu.sg/mankei/>).

$f : D' \rightarrow E'$  that can be measured on the image plane. Let  $\Pi : \mathcal{F} \rightarrow \mathcal{F}'$  be a linear operator that models the imaging system. Assume that  $\Pi$  is a low-pass filter with a bandwidth that can be normalized to a dimensionless number. In optical imaging, a fundamental mechanism of the low-pass filtering is the diffraction limit due to a finite numerical aperture [26]. For example,  $\Pi$  may be represented by the convolution

$$f(x) = \int_D h(x - X) F(X) d^m X, \quad F \in \mathcal{F}, \quad f \in \mathcal{F}'. \quad (1)$$

Common examples of the kernel  $h$  include the Gaussian  $h(x) \propto \exp(-x^2/2)$  and the sinc function  $h(x) \propto \text{sinc } x$ , defined as  $\text{sinc } x \equiv (\sin x)/x$  if  $x \neq 0$  and  $\text{sinc } 0 \equiv 1$ . If the domain  $D$  of the input function is assumed to be the whole Euclidean space  $\mathbb{R}^m$ , then elementary Fourier analysis shows that the frequency components of the input function outside the filter bandwidth are blocked or severely attenuated and cannot be observed from the output, especially if there is noise.

The overarching principle of superresolution imaging is to restrict the input function space  $\mathcal{F}$ , either by assumption or by experimental control, such that the low-pass filter is less harsh on the smaller function space and it becomes possible to measure certain object features with feature sizes somewhat smaller than the inverse of the filter bandwidth.

For convenience, I normalize the object-plane coordinate with respect to the filter bandwidth. Then, roughly speaking, a feature size is considered superresolution if it is somewhat smaller than 1. For example, if the object can be assumed to consist of a finite number of point sources, then there are only a finite number of unknown scalar parameters, and it becomes possible to estimate the source positions with superresolution precision by image processing, given a high enough SNR [27]. Studies in quantum metrology have also shown that judicious measurements can offer much better SNRs when observing certain superresolution features of a parametric model, such as the positions of a few point sources [3], [4], [5], [28] or the size of an object with a given shape [6], [29], [30].

To deal with more general objects, there is a need for a parameter space that is high-dimensional or even infinite-dimensional. When the parameter space is infinite dimensional, the estimation problem is called a semiparametric problem [31]. One of the first superresolution ideas that works under the semiparametric setting, as pioneered by Slepian, Bertero, and coworkers [15], [16], is to assume that the domain  $D$  of the input functions is bounded, such as  $[-\Delta, \Delta]$  with  $0 < \Delta < \infty$ , so that the low-pass filter is softer on those functions. To be precise, assume that  $\mathcal{F}$  and  $\mathcal{F}'$  are Hilbert spaces with the inner product denoted by  $\langle \cdot, \cdot \rangle$ . If  $\Pi$  is compact, it can be expressed as the singular-value decomposition (SVD)

$$\Pi F = \sum_{\mu} s_{\mu} b'_{\mu} \langle b_{\mu}, F \rangle, \quad F \in \mathcal{F}, \quad (2)$$

where  $\{s_{\mu}\}$  are a set of positive scalars called singular values and  $\{b_{\mu}\}$  and  $\{b'_{\mu}\}$  are called input and output singular functions, which are orthonormal subsets of  $\mathcal{F}$  and  $\mathcal{F}'$ , respectively. If  $D$  is bounded,  $\{b_{\mu}\}$  may be able to span  $L^2(D)$ , the Hilbert space of all square-integrable functions on  $D$ , meaning that all the functions in  $\mathcal{F} = L^2(D)$  can survive the filter. The input

signal can be decomposed in a (generalized) Fourier series as

$$F(X) = \sum_{\mu} \beta_{\mu} b_{\mu}(X), \quad \beta_{\mu} = \langle b_{\mu}, F \rangle. \quad (3)$$

Then, in the noiseless case, each Fourier coefficient  $\beta_{\mu}$  can be retrieved from the output function  $f = \Pi F$  by the linear filter

$$\beta_{\mu} = \frac{1}{s_{\mu}} \langle b'_{\mu}, f \rangle. \quad (4)$$

If noise is present in the output, the error of estimating each  $\beta_{\mu}$  depends on the magnitude of  $s_{\mu}$  relative to the noise level.

For many imaging problems in one dimension ( $D \subseteq \mathbb{R}$ ), each singular function with index  $\mu \in \mathbb{N}_0$  is an oscillatory function with  $\mu$  zeros within the domain, so the feature size of each singular function is roughly  $\Delta/(\mu+1)$ . A well known example is the prolate spheroidal functions for both  $\{b_{\mu}\}$  and  $\{b'_{\mu}\}$  when  $D = [-\Delta, \Delta]$  and  $h(x) \propto \text{sinc } x$  [15]. While the singular values stay nonzero for all  $\mu \in \mathbb{N}_0$ , they decrease rapidly with increasing  $\mu$  when  $\Delta/(\mu+1)$  becomes significantly smaller than 1, so superresolution is severely limited by the SNR in practice.

Kolobov and coworkers generalized this singular-system approach for coherent imaging in quantum optics by assuming that the input and output functions are the mean fields of certain quantum states, to be measured by homodyne detection in terms of the singular modes [18], [19], [20], [21]. They also proposed the use of a multimode squeezed state to reduce the noise, but it remains an open question how one can make an object emit the desired squeezed state in a real application.

More recently, Refs. [32], [33] have studied numerically the application of SPADE to incoherent imaging for general objects. Much work remains to be done, however, to understand and prove the advantage on a theoretical level.

The related idea of superdirectivity aims to produce an output electromagnetic field with superresolution features by controlling the input [34], [35]. Provided that the output singular functions  $\{b'_{\mu}\}$  of an electromagnetic system are also oscillatory within a bounded domain  $D'$ , superresolution in the output may be achieved by an input function  $F$  with Fourier coefficients  $\{\beta_{\mu}\}$  that are designed to compensate for the decay of the singular values  $\{s_{\mu}\}$ . Given the close relation between focusing and imaging [26], the superdirectivity concept can be exploited to give the point-spread function of an optical imaging system certain superresolution features by masking parts of the aperture [34], [35]. It is not at all clear, however, whether such a lossy imaging system can compete with other superresolution methods on statistical terms when noise is present.

The singular-system theory can be related to the phenomenon of superoscillation by considering the singular functions  $\{b_{\mu}\}$  and  $\{b'_{\mu}\}$  outside their bounded domains [1]. As  $\Pi$  is a low-pass filter when the function domains are taken to be the whole Euclidean space  $\mathbb{R}^m$ ,  $\{b_{\mu}\}$  and  $\{b'_{\mu}\}$  should also be bandlimited functions over  $\mathbb{R}^m$ , meaning that their fast oscillations within the bounded domains are necessarily accompanied by large sidelobes outside, as required for superoscillatory functions [1], [2].

For the arguably more important case of incoherent imaging,

Bertero and coworkers [16] considered the classical direct-imaging model

$$f(x) = \int_D |\psi(x - X)|^2 F(X) d^m X, \quad (5)$$

where  $F$  is the intensity of an object emitting spatially incoherent light,  $\psi$  is the point-spread function of a diffraction-limited imaging system with respect to the optical fields, and  $f$  is the intensity on the image plane [26]. Assuming that  $D$  is bounded or, more generally, that the object is illuminated by a focused beam with intensity  $I(X)$  such that  $f(x) = \int |\psi(x - X)|^2 F(X) I(X) d^m X$  in a confocal microscope, Bertero and coworkers proposed the processing of  $f$  based on the singular-system theory [16], via the use of intensity masks for example [17]. The proposal looks similar to the image-scanning microscopy proposed by Sheppard [36] and Müller and Enderlein [37], which also involves the processing of the image  $f$  to achieve modest superresolution, although the latter does not explicitly refer to the singular-system theory.

It is apparent from the preceding discussion that the SNR is a major concern for superresolution imaging, so it is desirable to minimize any unnecessary loss in the imaging system. It is also unclear which superresolution method performs the best statistically. This work proposes a measurement scheme that addresses these two issues: the scheme does not introduce any loss intentionally and its statistical performance in the presence of photon shot noise is close to the fundamental quantum limit imposed by quantum estimation theory [4], [5].

### III. KEY IDEAS

#### A. Proposal summary

I focus on one-dimensional paraxial imaging for simplicity ( $D \subseteq \mathbb{R}$ ) [26]. Let  $F(X)$  be the nonnegative object intensity function that is normalized as

$$\int_{-\infty}^{\infty} F(X) dX = 1. \quad (6)$$

Assume that the object size is subdiffraction—to be specific, assume

$$F(X) = 0 \text{ for } |X| > \Delta, \quad (7)$$

where  $0 < \Delta \ll 1$ . Such objects are, of course, abundant in astronomy, while the condition may also be enforced in microscopy by a confocal illumination with stimulated-emission depletion around a spot with size  $\Delta$  [22]. Apart from the assumptions above,  $F$  is assumed to be arbitrary, meaning that the problem is semiparametric. The goal of the proposal is to measure the Fourier coefficients

$$\beta_\mu = \int_{-\infty}^{\infty} b_\mu(X) F(X) dX, \quad (8)$$

where  $\{b_\mu : \mu \in \mathbb{N}_0\}$  are a set of orthonormal functions with respect to a certain inner product and each  $b_\mu(X)$  is oscillatory with  $\mu$  zeros in  $[-\Delta, \Delta]$ . The feature size of each  $b_\mu(X)$  function is then roughly  $\Delta/(\mu + 1)$ , which is much smaller than the diffraction-limited feature size on the order of 1.

The goal set forth is in the same spirit as the singular-system approach discussed in Sec. II, except that the basis  $\{b_\mu\}$  here does not come from a SVD. Rather, each  $b_\mu(X)$  is a polynomial

$$b_\mu(X) = \sum_{\nu=0}^{\mu} B_{\mu\nu} X^\nu, \quad (9)$$

such that each Fourier coefficient can be expressed as

$$\beta_\mu = \sum_{\nu=0}^{\mu} B_{\mu\nu} \theta_\nu, \quad (10)$$

where

$$\theta_\nu \equiv \int_{-\infty}^{\infty} X^\nu F(X) dX \quad (11)$$

is an object moment. As the object moments can be estimated efficiently by SPADE [6], [7], [8], [9], [10], each Fourier coefficient  $\beta_\mu$  of order  $\mu$  can be reconstructed from the object moments  $\{\theta_0, \theta_1, \dots, \theta_\mu\}$ .

The connection to superoscillation comes from the fact that, if one takes the whole  $\mathbb{R}$  to be the domain of  $F$ , the diffraction limit of the imaging system still imposes a bandwidth limit to each  $b_\mu(X)$ , so the oscillations of  $b_\mu(X)$  within  $[-\Delta, \Delta]$  should be accompanied by large sidelobes outside the interval.

As explained later, the actual  $b_\mu(X)$  functions implemented by the proposed method are only approximations of the desired polynomials, although the approximations can be quite accurate and still exhibit the desired oscillatory behaviors when  $\Delta \ll 1$ .

#### B. Orthogonal polynomials

Before explaining the proposal in further detail, it is necessary to introduce the concept of orthogonal polynomials first. It is helpful to perform a further normalization by writing

$$F(X) = \frac{1}{\Delta} W\left(\frac{X}{\Delta}\right), \quad (12)$$

where  $W$  is the object intensity function with a normalized width. Suppose that  $W$  can be expanded in a generalized Fourier series as

$$W(\xi) = \sum_{\mu=0}^{\infty} \beta_\mu a_\mu(\xi) R(\xi), \quad (13)$$

$$a_\mu(\xi) = \sum_{\nu=0}^{\mu} A_{\mu\nu} \xi^\nu, \quad (14)$$

where  $R(\xi)$  is a reference density, such as the rectangle function

$$R(\xi) = \frac{1_{|\xi| \leq 1}}{2}, \quad (15)$$

$$1_{\text{proposition}} \equiv \begin{cases} 1 & \text{if proposition is true,} \\ 0 & \text{otherwise,} \end{cases} \quad (16)$$

$\{a_\mu(\xi) : \mu \in \mathbb{N}_0\}$  are the orthonormal polynomials with respect to the real  $R$ -weighted inner product [38]

$$\langle a_\mu(\xi), a_\nu(\xi) \rangle_{R(\xi)} \equiv \int_{-\infty}^{\infty} a_\mu(\xi) a_\nu(\xi) R(\xi) d\xi = \delta_{\mu\nu}, \quad (17)$$

and each  $\beta_\mu \in \mathbb{R}$  is a Fourier coefficient that can also be expressed as

$$\beta_\mu = \int_{-\infty}^{\infty} a_\mu(\xi) W(\xi) d\xi = \int_{-\infty}^{\infty} a_\mu\left(\frac{X}{\Delta}\right) F(X) dX. \quad (18)$$

The coefficient matrix  $A$  in Eq. (14) can be derived by applying the Gram-Schmidt procedure to the monomials  $\{1, \xi, \xi^2, \dots\}$ . The procedure implies the property

$$\langle a_\mu(\xi), \xi^\nu \rangle_{R(\xi)} = 0 \text{ for } \mu > \nu \in \mathbb{N}_0, \quad (19)$$

which will be useful throughout this paper. The desired  $B$  coefficients in Eqs. (9) and (10) become

$$B_{\mu\nu} = \frac{A_{\mu\nu}}{\Delta^\nu}. \quad (20)$$

For example, for the rectangle  $R$  given by Eq. (15), the orthonormal polynomials are given by

$$a_\mu(\xi) = \sqrt{2\mu + 1} P_\mu(\xi), \quad (21)$$

where  $\{P_\mu : \mu \in \mathbb{N}_0\}$  are the Legendre polynomials [38]. Each  $a_\mu(X/\Delta)$  is an oscillatory function with  $\mu$  zeros within the subdiffraction region  $|X| \leq \Delta$ . To illustrate, Fig. 1 plots the monomials  $\xi^\mu$  and the orthogonal polynomials given by Eq. (21) up to  $\mu = 8$ .

### C. Moment measurement and Fourier analysis by spatial-mode demultiplexing (SPADE)

The measurement of object moments by SPADE has been extensively studied in the context of quantum-inspired imaging [6], [7], [8], [9], [10], [12], [11], [13], [14]. The relation between the moments and the Fourier coefficients given by Eq. (10) is a helpful insight in bridging the literature on moment estimation to other areas of superresolution research, as the concept of resolution in optics is commonly framed in terms of Fourier analysis [1], [26], and the relation between resolution and the moments is less clear. Here I review the principle of SPADE and discuss how it can be used to learn the Fourier coefficients.

Let  $\psi(x)$  be the complex-valued point-spread function of a diffraction-limited imaging system for the optical field, where  $x \in \mathbb{R}$  is the image-plane coordinate that is normalized with respect to the magnification factor [26] and the function is normalized as  $\int_{-\infty}^{\infty} |\psi(x)|^2 dx = 1$ . The optical transfer function, defined as

$$\Psi(k) \equiv \frac{1}{\sqrt{2\pi}} \int_{-\infty}^{\infty} \psi(x) \exp(-ikx) dx, \quad (22)$$

is assumed to have a finite width; common examples in optics include the Gaussian

$$\Psi(k) = \left(\frac{2}{\pi}\right)^{1/4} \exp(-k^2), \quad (23)$$

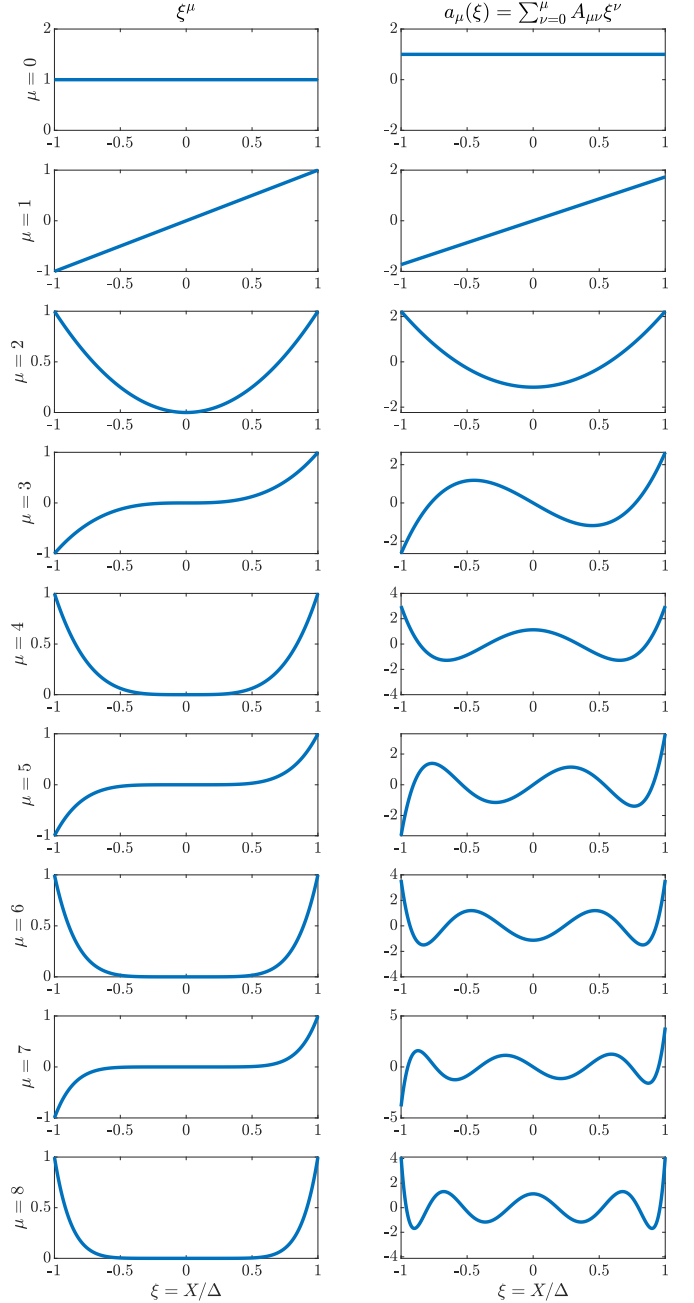


Fig. 1. Left column: plots of monomials  $\xi^\mu$  from  $\mu = 0$  to  $\mu = 8$ . Right column: plots of the orthogonal polynomials  $a_\mu(\xi)$  given by Eq. (21). As each orthogonal polynomial  $a_\mu(\xi)$  of order  $\mu$  can be constructed from the monomials  $\{\xi^\nu : \nu = 0, 1, \dots, \mu\}$ , it follows that each Fourier coefficient  $\beta_\mu = \int_{-\infty}^{\infty} a_\mu(X/\Delta) F(X) dX$  can be constructed from the moments  $\{\theta_\nu = \int_{-\infty}^{\infty} X^\nu F(X) dX : \nu = 0, 1, \dots, \mu\}$ .



and the rectangle

$$\Psi(k) = \frac{1_{|k| \leq 1}}{\sqrt{2}}. \quad (24)$$

With direct imaging, which measures the intensity on the image plane with an image sensor, the expected image intensity is proportional to [26], [39]

$$f(x) \equiv \int_{-\infty}^{\infty} |\psi(x - X)|^2 F(X) dX. \quad (25)$$

The SPADE scheme put forth, on the other hand, processes the image-plane light by further photonics before photodetection. In the scheme, the light is first demultiplexed in terms of the point-spread-function-adapted (PAD) basis  $\{\phi_q(x) : q \in \mathbb{N}_0\}$  [40], [7], where each PAD mode is defined as

$$\phi_q(x) \equiv \frac{(-i)^q}{\sqrt{2\pi}} \int_{-\infty}^{\infty} \Psi(k) g_q(k) e^{ikx} dk \quad (26)$$

and  $g_q(k)$  is an orthonormal polynomial with respect to the  $|\Psi|^2$ -weighted inner product

$$\langle g_q(k), g_p(k) \rangle_{|\Psi(k)|^2} \equiv \int_{-\infty}^{\infty} g_q^*(k) g_p(k) |\Psi(k)|^2 dk = \delta_{qp}. \quad (27)$$

For example, if  $\Psi(k)$  is the Gaussian given by Eq. (23), then

$$g_q(k) = \frac{1}{\sqrt{q!}} \text{He}_q(2k), \quad (28)$$

where  $\{\text{He}_q : q \in \mathbb{N}_0\}$  are the probabilist's Hermite polynomials [38], or if  $\Psi(k)$  is the rectangle given by Eq. (24), then

$$g_q(k) = \sqrt{2q+1} P_q(k). \quad (29)$$

The orthonormality of the orthogonal polynomials implies the orthonormality of the PAD basis with respect to the inner product for the optical fields, viz.,

$$\langle \phi_q, \phi_p \rangle \equiv \int_{-\infty}^{\infty} \phi_q^*(x) \phi_p(x) dx = \langle g_q, g_p \rangle_{|\Psi|^2} = \delta_{qp}. \quad (30)$$

As the image-plane optical fields are spanned by

$$\{\psi_X : \psi_X(x) = \psi(x - X), |X| \leq \Delta\}, \quad (31)$$

the identity

$$\sum_{q=0}^{\infty} |\langle \phi_q, \psi_X \rangle|^2 = 1 \quad \forall |X| \leq \Delta \quad (32)$$

implies that all the image-plane photons can be captured in the PAD basis and the demultiplexer can be lossless, at least in principle. The identity can be proved for any  $\Psi$  that satisfies  $\int_{-\infty}^{\infty} \exp(c|k|) |\Psi(k)|^2 dk < \infty$  for some  $c > 0$  by writing

$$\langle \phi_q, \psi_X \rangle = i^q \langle g_q(k), e^{-ikX} \rangle_{|\Psi(k)|^2}, \quad (33)$$

noting that the orthogonal polynomials  $\{g_q\}$  are complete in the  $L_2(|\Psi|^2)$  space for the assumed class of  $\Psi$ , and applying Parseval's identity [41].

Although only a finite number of modes may be demultiplexed in practice, physical intuition suggests that the coupling

efficiency from a subdiffraction object to a PAD mode should decrease rapidly with increasing mode order, and a truncation of the demultiplexed modes should not have a major impact on the total photon-collection efficiency.

After the demultiplexer, the light passes through pairwise interferometers before photon counting, as depicted in Fig. 2. The expected value ( $\mathbb{E}$ ) of each photon count is

$$\mathbb{E}(n_q^\pm) = N f_q^\pm, \quad q \in \mathbb{N}_0, \quad (34)$$

$$f_q^\pm \equiv \frac{1}{2} \int_{-\infty}^{\infty} h_q^\pm(X) F(X) dX, \quad (35)$$

$$h_q^\pm(X) \equiv \left| \left\langle \frac{\phi_q \pm \phi_{q+1}}{\sqrt{2}}, \psi_X \right\rangle \right|^2, \quad (36)$$

where  $N$  is the expected photon number detected in all outputs and  $h_q^\pm(X)$  is a transition probability of each photon reaching an output as a function of the point-source displacement  $X$ . Note that all the  $h_q^\pm(X)$  functions are bandlimited because of the bandlimited  $\psi_X$  and  $\phi_q$ , so each  $\mathbb{E}(n_q^\pm)$  is, in effect, the outcome of passing  $F(X)$  through a linear bandlimited filter.

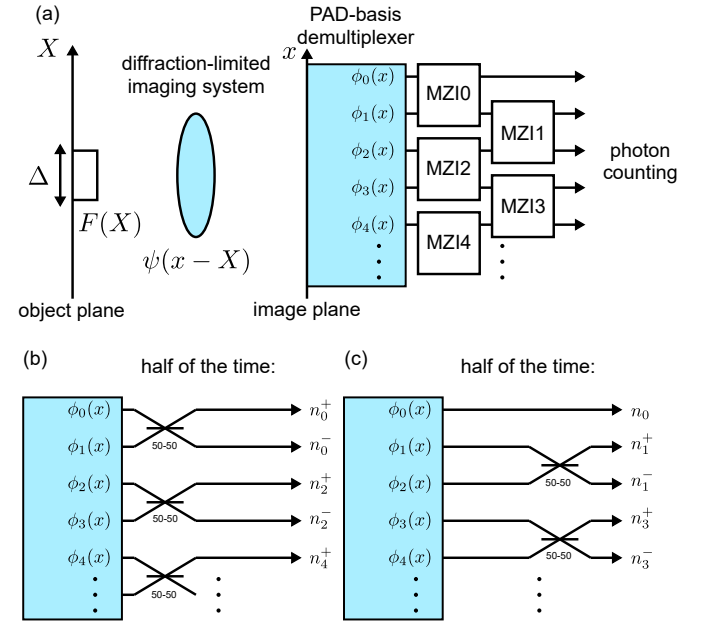


Fig. 2. The proposed SPADE scheme to measure the object moments and the Fourier coefficients for a distribution of incoherent sources. (a) Basic setup, where  $F(X)$  is the object intensity function,  $\Delta$  is the object width, and  $\psi(x - X)$  is the point-spread function of the imaging system for the optical field. The demultiplexer sorts the image-plane light in terms of the point-spread-function-adapted (PAD) basis  $\{\phi_q(x)\}$ , and each Mach-Zehnder interferometer (MZI) further combines a pair of the outputs. Each MZI operates as a variable beamsplitter by having a phase modulator that controls the relative phase between the two arms. (b) Configuration of the MZIs for half of the observation time: MZI0, MZI2, ... should be set as 50-50 beamsplitters, while MZI1, MZI3, ... should be set as passthroughs. (c) Configuration for the other half of the time: MZI0, MZI2, ... should be set as passthroughs, while MZI1, MZI3, ... should be set as 50-50 beamsplitters.  $n_q^\pm$  and  $n_0$  are the photon counts that should be further processed to produce estimates of the moments and the Fourier coefficients. The expected photon counts are given by Eqs. (34)–(36), while the estimators for the Fourier coefficients and the moments are given by Eqs. (42) and (43).

The setup enables both even and odd moments to be measured; without the interferometers, only even moments can be measured [7]. To see this, note that, since  $\exp(-ikX) =$

$\sum_p (-ikX)^p/p!$  and  $\langle g_q(k), k^p \rangle_{|\Psi(k)|^2} = 0$  for  $p < q$ , the transition amplitude for each demultiplexer output given by Eq. (33) becomes

$$\langle \phi_q, \psi_X \rangle \sim H_q X^q - iH'_q X^{q+1}, \quad (37)$$

where  $H_q \equiv \langle g_q(k), k^q \rangle_{|\Psi(k)|^2}/q!$  and  $H'_q \equiv \langle g_q(k), k^{q+1} \rangle_{|\Psi(k)|^2}/(q+1)!$  are real constants and  $\sim$  means identical in the leading order for  $|X| \leq \Delta \ll 1$ . The transition probability given by Eq. (36) becomes

$$h_q^\pm(X) \sim \frac{H_q^2}{2} X^{2q} \pm H_q H_{q+1} X^{2q+1}, \quad (38)$$

the expected photon count becomes

$$\mathbb{E}(n_q^\pm) \sim \frac{N}{2} \left( \frac{H_q^2}{2} \theta_{2q} \pm H_q H_{q+1} \theta_{2q+1} \right), \quad (39)$$

where each  $\theta_\nu$  is an object moment defined by Eq. (11), and the addition and subtraction of the photon counts give

$$\mathbb{E}(n_q^+ + n_q^-) \sim \frac{NH_q^2}{2} \theta_{2q}, \quad (40)$$

$$\mathbb{E}(n_q^+ - n_q^-) \sim NH_q H_{q+1} \theta_{2q+1}. \quad (41)$$

Thus, the outputs  $n_q^+ \pm n_q^-$  can be used to estimate the moments  $\theta_{2q}$  and  $\theta_{2q+1}$ , and the moment estimates can then be plugged into Eq. (10) to estimate the Fourier coefficients.

To be more precise about the counting statistics, assume that the photon counts are independent and Poisson random variables, which are an excellent assumption for natural or fluorescent sources at optical frequencies [4], [22], [39], [42]. Assume also that  $N$  is unknown, for generality. Let the total photon number detected in all outputs be  $L$ . Conditioned on  $L$ , the count statistics become multinomial. Then an estimator of  $\beta_\mu$  can be constructed as follows:

$$\tilde{\beta}_\mu = \sum_{\nu=0}^{\mu} \frac{A_{\mu\nu}}{\Delta^\nu} \tilde{\theta}_\nu, \quad (42)$$

$$\tilde{\theta}_\nu = \begin{cases} 1, & \nu = 0, \\ (n_q^+ - n_q^-)/(LH_q H_{q+1}), & \nu \text{ odd}, \nu = 2q + 1, \\ 2(n_q^+ + n_q^-)/(LH_q^2), & \nu \text{ even}, \nu = 2q. \end{cases} \quad (43)$$

For a given  $L$ ,  $\mathbb{E}(n_q^\pm) = L f_q^\pm = L \int_{-\infty}^{\infty} h_q^\pm(X) F(X) dX$ , and the expected value of  $\tilde{\beta}_\mu$  can be expressed as

$$\mathbb{E}(\tilde{\beta}_\mu) = \int_{-\infty}^{\infty} b_\mu(X) F(X) dX, \quad (44)$$

where  $b_\mu(X)$  is a filter function that should approximate the oscillatory  $a_\mu(X/\Delta)$  in the region  $|X| \leq \Delta$ . As  $b_\mu(X)$  is a linear combination of the bandlimited  $h_q^\pm(X)$  functions, it should be a superoscillatory function with large sidelobes; Fig. 3 supports this assertion by plotting  $b_\mu(X)$  for  $\mu = 1, 2, \dots, 8$ . The filter functions also resemble the prolate-spheroidal functions that are well known in superresolution theory [1].

Note that each  $\tilde{\beta}_\mu$  involves PAD modes up to order  $q = \lceil \mu/2 \rceil$  only, so the estimation of each Fourier coefficient requires the demultiplexing of only a finite number of modes. The efficiency of a subdiffraction object coupling into a PAD

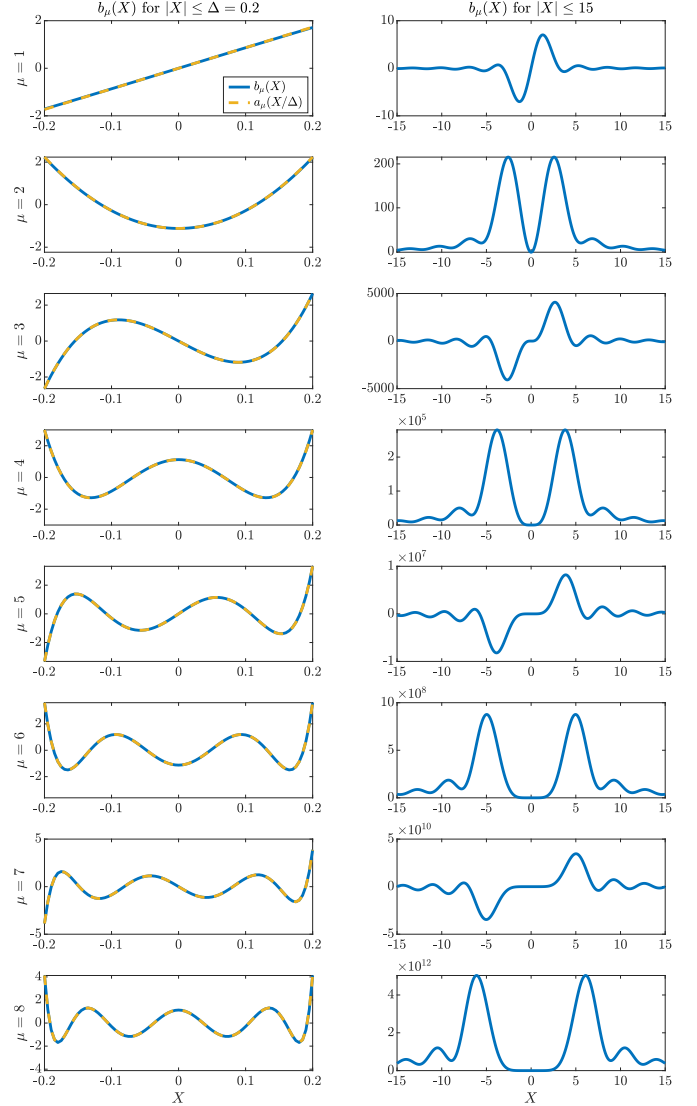


Fig. 3. Left column: plots of the exact filter function  $b_\mu(X)$  (solid blue lines) from  $\mu = 1$  to  $\mu = 8$ , as defined by Eqs. (42)–(44) and implemented by the measurement in Fig. 2, with the estimators given by Eqs. (42) and (43). The functions are seen to be close to the desired filters  $a_\mu(X/\Delta)$  (dash yellow lines). Right column: plots of  $b_\mu(X)$  for a wider range of  $X$ , showing the large sidelobes. The plots assume that  $\Delta = 0.2$ ,  $R(\xi)$  is the rectangle function given by Eq. (15),  $\{a_\mu(\xi)\}$  are the Legendre polynomials given by Eq. (21),  $\Psi(k)$  is the rectangle function given by Eq. (24),  $\{g_q(k)\}$  are the Legendre polynomials given by Eq. (29), and the  $b_\mu$  functions are computed using Eqs. (42), (43), and (34)–(36). To compare the feature sizes here with the diffraction limit, note that direct imaging according to Eq. (25) completely blocks any sinusoidal component  $\exp(i\kappa X)$  of the input function  $F(X)$  when  $\mathbb{R}$  is the function domain and  $|\kappa| \geq 2$ , so a diffraction-limited feature size can be defined as the period  $2\pi/|\kappa| = \pi$ , which is much larger than the feature sizes of the oscillations shown in the left column.

mode is expected to go down for higher mode orders, so there are only a finite number of modes that offer useful SNRs and a finite number of Fourier coefficients that can be estimated accurately in practice.

Note also that the moment estimator given by Eq. (43) is based on a Taylor-series approximation made in Eqs. (37)–(41), so the estimator is unbiased only in the leading order ( $\mathbb{E}(\hat{\theta}_\nu) \sim \theta_\nu$ ). Since the  $b_\mu(X)$  filter function defined by Eqs. (42)–(44) is exactly equal to the orthogonal polynomial  $a_\mu(X/\Delta)$  only when the moment estimator is exactly unbiased ( $\mathbb{E}(\hat{\theta}_\mu) = \theta_\mu$ ), the implemented  $b_\mu(X)$ , as plotted in Fig. 3 for example, is only an approximation of  $a_\mu(X/\Delta)$ . The bias can be reduced by measuring more modes and using a more complicated moment estimator [9], although Fig. 3 shows that  $b_\mu(X)$  and  $a_\mu(X/\Delta)$  can be very close to begin with and the  $b_\mu(X)$  functions still exhibit the desired oscillatory behaviors.

#### D. Implementations of SPADE

The PAD-basis demultiplexer is the key component in the proposed scheme. Also known as a mode sorter in other areas of optics, the demultiplexer can be implemented by many different methods, as reviewed in Refs. [4], [43]. I mention only a few implementations that have recently been demonstrated for the purpose of superresolution:

- 1) Multi-plane light conversion (MPLC) [44], which involves light propagation through a series of specially designed phase plates. With this device, the outputs are well separated Gaussian beams and can be coupled into single-mode fibers, so the MZIs can be implemented using standard components. There also exist algorithms to design the phase plates for more general unitary operations [45], [46].
- 2) Super-resolved position localization by inversion of coherence along an edge (SPlice) [47], [13], which involves a binary phase plate and a single-mode fiber to perform mode selection.
- 3) Mode-selective up-conversion [48], [49], [50], which involves an optical pump with an appropriate spatial or temporal profile to up-convert the desired mode of the input via sum frequency generation in a nonlinear medium.
- 4) Image-inversion interferometry [51], [52], which involves a Mach-Zehnder interferometer that inverts the spatial profile of the optical beam in one of the arms.
- 5) Mode-selective heterodyne detection [11], [53], which involves the interference of the input with a local oscillator with an appropriate spatial profile at an image sensor.

It is beyond the scope of this work to discuss the experimental details and the relative merits of different implementations. Here I only emphasize the general fact that, even though SPADE is by no means trivial to implement experimentally, it requires only known and accessible optical materials and technologies.

It is interesting to note that coronagraphs [54] and nulling interferometers [55] in astronomy turn out to perform mode sorting not unlike some simple versions of SPADE, although

their superiority to direct imaging in rigorous statistical terms, their quantum optimality, and their applicability to more general imaging problems do not seem to have been studied before. The practical success of those instruments in astronomy offers encouragement that more advanced indirect imaging methods such as SPADE should remain viable in realistic conditions and in applications beyond astronomy.

#### E. Possible generalizations

If the demultiplexer is not placed on an image plane, the wavefunctions of the modes to be demultiplexed should be modified. Let  $\alpha_X(x)$  be the optical field on a certain plane after the aperture produced by a point source with displacement  $X$  and suppose that the field on that plane is to be demultiplexed. In principle, the image-plane  $\psi_X$  is related to  $\alpha_X$  by a unitary operator  $U$  that models the propagation through the optical components between the two planes [26], viz.,

$$\psi_X(x) = (U\alpha_X)(x) = \int_{-\infty}^{\infty} U(x, x')\alpha_X(x')dx'. \quad (45)$$

Then the preceding theory still holds if the wavefunctions of the PAD modes are modified by the adjoint operator  $U^\dagger$  (which is also unitary), such that

$$\langle U^\dagger\phi_q, \alpha_X \rangle = \langle \phi_q, U\alpha_X \rangle = \langle \phi_q, \psi_X \rangle, \quad (46)$$

and the transition amplitude for each demultiplexer output is still given by Eq. (33). In other words, to compute the wavefunctions of the modes to be demultiplexed, one simply backpropagates the wavefunctions of the PAD modes from the image plane to the desired input plane of the demultiplexer, as illustrated by Fig. 4.

The theory here can be applied to imaging with multiple apertures, such as multi-telescope interferometry [56], by specifying an optical transfer function  $\Psi(k)$  that models the total aperture. Each PAD mode is then a “supermode” that is a superposition of optical fields from all the apertures, and the demultiplexer would require a more elaborate optical processor that combines them coherently.

The performance of the proposed scheme may be improved further by optimizing the interferometry and the time allocation between the interferometer settings, although Sec. IV-C later shows that the present scheme is already quantum-optimal in terms of its error scaling with the object size.

Regardless of the object size  $\Delta$ , unbiased estimators of the moments, and therefore the Fourier coefficients, may still be constructed from the outputs of the proposed SPADE scheme [4]. If  $\Delta$  is not subdiffraction, however, it becomes unclear whether SPADE offers a statistical advantage over direct imaging. Moreover, as the efficiency of coupling to a higher-order mode becomes higher for a larger object, more modes will acquire significant photon numbers and will need to be measured in order to minimize the bias of the estimators.

Generalizations for imaging in two dimensions and spectroscopy are also possible by following Refs. [7], [50], [57].

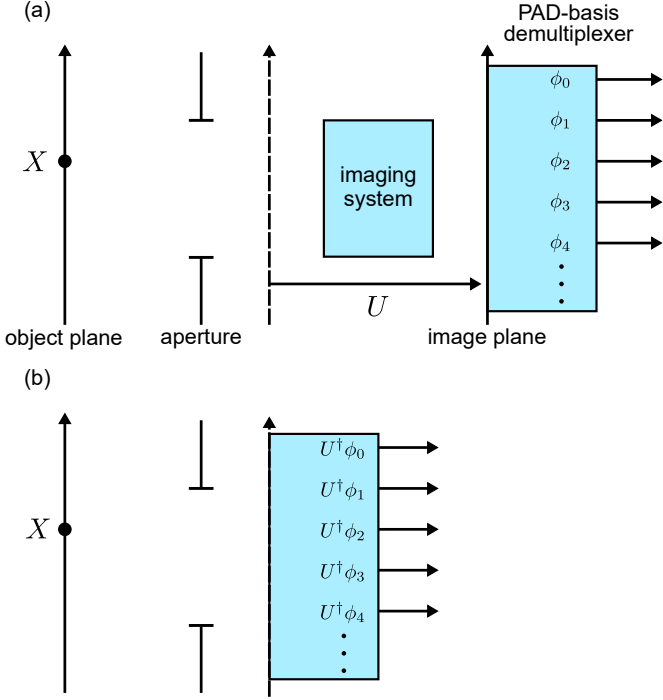


Fig. 4. (a) In the original proposal, demultiplexing in terms of the PAD basis is applied to the image-plane light. The optical field on the image plane can be related to the field on another plane after the aperture by a unitary operator  $U$ . (b) If demultiplexing is applied on that plane, the same results in the original proposal can be reproduced by modifying the basis via the adjoint operator  $U^\dagger$ .

#### IV. STATISTICAL ANALYSIS

##### A. Error with SPADE

Although the sidelobes of the filter functions are large for a subdiffraction object size  $\Delta$ , they occur for larger  $X$  and are irrelevant to an object of subdiffraction size. Of more fundamental concern is the estimation error. Assume  $\Delta \ll 1$  and the asymptotic notations  $O[p(\Delta)]$  (order at most  $p(\Delta)$ ),  $\Omega[p(\Delta)]$  (order at least  $p(\Delta)$ ), and  $\Theta[p(\Delta)]$  (order exactly  $p(\Delta)$ ) for  $\Delta \rightarrow 0$  [58]. With multinomial statistics and

$$f_q^\pm = \Theta(\Delta^{2q}), \quad (47)$$

the variance ( $\mathbb{V}$ ) of  $\tilde{\beta}_\mu$  can be expressed as

$$\begin{aligned} \mathbb{V}(\tilde{\beta}_\mu) &\sim \frac{(A_{\mu\mu})^2}{\Delta^{2\mu}} \mathbb{V}(\tilde{\theta}_\mu) = \frac{(A_{\mu\mu})^2}{\Delta^{2\mu}} \frac{\Theta(\Delta^{2\lceil\mu/2\rceil})}{L} \\ &= \frac{\Theta(\Delta^{-2\lceil\mu/2\rceil})}{L}, \end{aligned} \quad (48)$$

Unfortunately—but perhaps unsurprisingly—the error gets worse for smaller  $\Delta$ , especially for higher  $\mu$ . The achievable resolution enhancement, in terms of the number of accurately estimated Fourier coefficients, depends on  $\Delta$  and the photon budget  $N = \mathbb{E}(L)$ .

##### B. Comparison with the Cramér-Rao bounds (CRBs) for direct imaging

The superiority of the proposed SPADE scheme over any processing of the image-plane intensity can be proved by comparing the error of the former with a Cramér-Rao bound

(CRB) for direct imaging [4]. Ideal direct imaging can be modeled as a measurement of a spatial Poisson process with the intensity function  $Nf(x)$ , where  $f(x)$  is given by Eq. (25) [39]. The parameter space is assumed here to be the set of all probability densities for  $F(X)$ , while the Fourier coefficient  $\beta_\mu[F]$  given by Eq. (44) is taken as the parameter of interest.

If the point-spread function  $|\psi(x)|^2$  is Gaussian, the exact CRB for semiparametric moment estimation with direct imaging can be derived using the techniques in Refs. [7], [9], [31], despite the infinite dimensionality of the parameter space. Furthermore, there exists an efficient unbiased estimator that attains the bound [9]. As each Fourier coefficient  $\beta_\mu$  is a linear combination of the moments, it is straightforward to derive the CRB for each  $\beta_\mu$  from the results in Refs. [7], [9]. Conditioned on the total photon number  $L$ , the CRB is

$$\text{MSE}^{(\text{direct})} \geq \mathcal{C}^{(\text{direct})} = \frac{1}{L} \left[ BC^{-1} M (C^{-1})^\top B^\top \right]_{\mu\mu} \quad (49)$$

$$= \frac{\Theta(\Delta^{-2\mu})}{L}, \quad (50)$$

where  $\text{MSE}^{(\text{direct})}$  is the mean-square error of direct imaging with any unbiased estimator of  $\beta_\mu$ ,  $M$  is the image moment matrix given by

$$M_{uv} \equiv \langle x^u, x^v \rangle_{f(x)} - \langle x^u, 1 \rangle_{f(x)} \langle x^v, 1 \rangle_{f(x)}, \quad u, v \in \mathbb{N}_0, \quad (51)$$

$B$  and  $C$  are lower-triangular matrices given by

$$C_{uv} \equiv 1_{u \geq v} \binom{u}{v} \int_{-\infty}^{\infty} x^{u-v} |\psi(x)|^2 dx, \quad (52)$$

$$B_{uv} \equiv 1_{u \geq v} \frac{A_{uv}}{\Delta^v}, \quad (53)$$

and  $\top$  denotes the transpose. By virtue of the lower-triangularity of  $B$  and  $C$ , only the submatrices of  $B$ ,  $C$ , and  $M$  with entries up to  $u = v = \mu$  are needed to compute  $\mathcal{C}^{(\text{direct})}$ . A comparison of Eq. (48) with Eq. (50) suggests that SPADE is superior to direct imaging for  $\mu \geq 2$ .

If  $|\psi(x)|^2$  is not Gaussian, the exact semiparametric CRB is much more difficult to derive. An alternative CRB can be obtained via the parametric-submodel approach in Ref. [10]. It involves the judicious choice of an unfavorable parametric submodel  $F_\vartheta(X)$  with a scalar parameter  $\vartheta \in \mathbb{R}$  and  $F_0(X)$  being set as the true object intensity. Then the CRB of the submodel, denoted as  $\tilde{\mathcal{C}}^{(\text{direct})}$ , is a lower bound on the exact CRB  $\mathcal{C}^{(\text{direct})}$  for the semiparametric problem [31], viz.,

$$\mathcal{C}^{(\text{direct})} \geq \tilde{\mathcal{C}}^{(\text{direct})}. \quad (54)$$

This lower bound makes intuitive sense, as the submodel assumes fewer unknown parameters and should therefore permit a lower uncertainty in the parameter of interest. Conditioned on  $L$ , the submodel CRB can be expressed as

$$\tilde{\mathcal{C}}^{(\text{direct})} = \frac{(\partial \beta_\mu)^2}{LJ}, \quad \partial \beta_\mu \equiv \left. \frac{\partial \beta_\mu[F_\vartheta]}{\partial \vartheta} \right|_{\vartheta=0}, \quad (55)$$

where  $\partial$  denotes the partial derivative at the true  $\vartheta = 0$  and  $J$  is the per-photon Fisher information for the submodel. Since the parameter space consists of all probability densities, there is considerable freedom in specifying a submodel. A



convenient one is [31]

$$F_{\vartheta}(X) = \frac{\{1 + \tanh[\vartheta c_{\mu}(X/\Delta)]\} F_0(X)}{\int_{-\infty}^{\infty} (\text{numerator}) dX}, \quad (56)$$

where  $c_{\mu}$  satisfies the zero-mean condition  $\int_{-\infty}^{\infty} c_{\mu}(X/\Delta) F_0(X) dX = 0$  at the truth, such that

$$\partial F_{\vartheta}(X) = c_{\mu} \left( \frac{X}{\Delta} \right) F_0(X). \quad (57)$$

Since  $F_0(X)$  is assumed to coincide with the true density and  $F_{\vartheta}(X)$  is a valid probability density for any  $\vartheta \in \mathbb{R}$ , Eq. (56) satisfies the requirements of a parametric submodel for any zero-mean  $c_{\mu}$ , and the CRB computed from the submodel can be used in Eq. (54). The choice of an unfavorable submodel then boils down to the choice of  $c_{\mu}$ . A fruitful choice of  $c_{\mu}$  made in Ref. [10] is an orthogonal polynomial with respect to the true  $W(\xi) = W_0(\xi)$ , which is defined by  $F_0(X) = \Delta^{-1} W_0(X/\Delta)$  in the same manner as Eq. (12), while  $\mu$  is chosen to match that of  $\beta_{\mu}$ . Then

$$\partial \beta_{\mu} = \int_{-\infty}^{\infty} a_{\mu} \left( \frac{X}{\Delta} \right) c_{\mu} \left( \frac{X}{\Delta} \right) F_0(X) dX \quad (58)$$

$$= A_{\mu\mu} \langle \xi^{\mu}, c_{\mu}(\xi) \rangle_{W_0(\xi)} = \Theta(1). \quad (59)$$

The Fisher information, on the other hand, is given by

$$J = \int_{-\infty}^{\infty} \frac{[\partial f_{\vartheta}(x)]^2}{f_0(x)} dx, \quad (60)$$

$$f_{\vartheta}(x) \equiv \int_{-\infty}^{\infty} |\psi(x - X)|^2 F_{\vartheta}(X) dX. \quad (61)$$

Although the submodel CRB is a valid lower bound on the MSE for the semiparametric problem, it is difficult to know how much looser it is than the exact bound.

Even with the submodel approach, the scaling of the CRB with respect to  $\Delta$  is difficult to derive if the point-spread function  $|\psi(x)|^2$  contains zeros [10]. I therefore resort to numerics to compute the submodel bound here. The final numerical results are plotted in Fig. 5. The figure plots the variance of the estimator of  $\beta_{\mu}$  ( $\mu = 1, 2, 3$ ) with SPADE and the CRBs for direct imaging against the object size  $\Delta$  in log-log scale, assuming that the true object intensity is

$$F(X) = F_0(X) = \frac{1_{|X| \leq \Delta}}{2\Delta}. \quad (62)$$

The left column assumes a Gaussian optical transfer function with  $\Psi(k)$  given by Eq. (23), while the right column assumes the rectangle function given by Eq. (24). The caption of Fig. 5 contains further details about the numerical analysis.

A comparison of the SPADE error given by Eq. (48) and the CRB given by Eq. (50) suggests that SPADE has an advantage only for  $\mu \geq 2$ , and indeed Fig. 5 supports this suggestion. For  $\mu = 1$  (first row of Fig. 5), the direct-imaging CRBs are somewhat lower than the SPADE error, while the scalings with respect to  $\Delta$  all roughly follow Eqs. (48) and (50). The gap may be partially attributed to the fact that SPADE uses only half of the time to obtain the photon count  $n_0^-$  that contributes to  $\tilde{\theta}_1$  and  $\tilde{\beta}_1$ .

For  $\mu = 2, 3$  (second and third rows of Fig. 5), SPADE

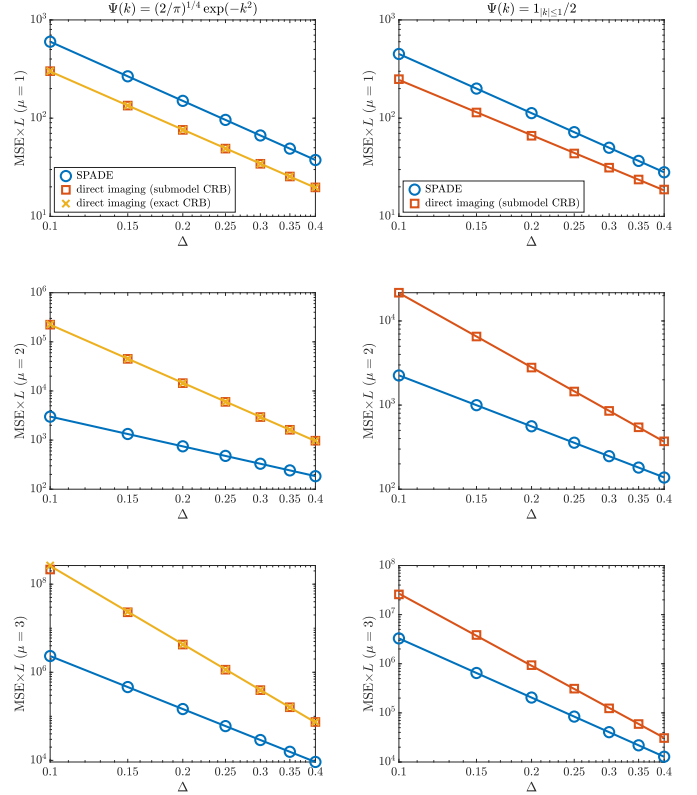


Fig. 5. A numerical comparison of the SPADE errors with the CRBs for direct imaging in estimating the Fourier coefficients  $\beta_{\mu}$ ,  $\mu = 1, 2, 3$ , assuming that the true object intensity is given by Eq. (62). In each plot of log-log scale, the vertical axis is the mean-square error (MSE) multiplied by the photon number  $L$ , while the horizontal axis is the object size  $\Delta$  normalized with respect to the point-spread-function width. All the quantities are dimensionless by definition. The SPADE error is the variance of the estimator given by Eqs. (42) and (43), assuming multinomial statistics for  $\{n_q^{\pm}\}$  with a photodetection probability distribution given by Eqs. (35) and (36). For direct imaging, the exact semiparametric CRB is the  $\tilde{C}^{(\text{direct})}$  given by Eqs. (49)–(53), while the submodel CRB is the  $\tilde{C}^{(\text{direct})}$  given by Eqs. (55)–(61) and computed numerically by discretizing the integrals in those equations. The left column assumes the Gaussian transfer function given by Eq. (23), while the right column assumes the rectangle  $\Psi(k)$  given by Eq. (24), in which case the exact CRB for direct imaging is unknown and only the submodel CRB is plotted. The straight lines are least-squares linear fits of log MSE versus log  $\Delta$  and log CRB versus log  $\Delta$  (assuming the exact CRB for the left column); their slopes differ from the corresponding theoretical exponents in Eqs. (48), (50), and (63) by at most a fractional error of 7% only, where the fractional error is defined as  $|\text{slope} - \text{theoretical exponent}| / |\text{theoretical exponent}|$ .

begins to show a substantial advantage. The scalings of the SPADE error again follow Eq. (48), while the scalings of the direct-imaging CRBs follow Eq. (50) for the Gaussian  $\Psi(k)$  (left column of Fig. 5). On a side note, it is fortuitous here that the submodel CRB is so close to the exact CRB for the Gaussian case, meaning that the chosen submodel happens to be close to the least favorable submodel that gives the exact CRB [31].

For the rectangle  $\Psi(k)$ , the point-spread function  $|\psi(x)|^2 \propto \text{sinc}^2 x$  contains zeros, which may enhance the submodel Fisher information for direct imaging given by Eq. (60) by a  $\Theta(\Delta^{-1})$  factor [59]. The plots of the submodel CRB in the right column of Fig. 5 and the arguments in Ref. [59] motivate the conjecture that, when  $|\psi(x)|^2$  contains zeros, the submodel

CRB for direct imaging obeys the scaling

$$\tilde{C}^{(\text{direct})} = \begin{cases} \frac{\Theta(\Delta^{-2})}{L}, & \mu = 1, \\ \frac{\Theta(\Delta^{-2\mu+1})}{L}, & \mu \geq 2, \end{cases} \quad (63)$$

although the tightness of this submodel bound for the semi-parametric problem remains unclear.

### C. Quantum Cramér-Rao bounds (QCRBs)

The parametric-submodel approach can also be used to compute a quantum CRB  $\tilde{H}$  that is valid for any measurement [10]. The result is

$$\text{MSE} \geq C \geq H \geq \tilde{H} = \frac{(\partial \beta_\mu)^2}{NK} = \frac{\Omega(\Delta^{-2\lceil \mu/2 \rceil})}{N}, \quad (64)$$

where MSE is now the mean-square error of any unbiased estimator,  $C$  is the classical CRB for any measurement of the image-plane light,  $H$  is the exact QCRB for the semiparametric problem [60], and  $\tilde{H}$  is the QCRB for the submodel. The scaling

$$K = O(\Delta^{2\lceil \mu/2 \rceil}) \quad (65)$$

of the Helstrom information  $K$  [5] for the submodel is proved in Ref. [10]. With the detected photon number  $L$  being close to the expected value  $N$  for large  $N$ , the SPADE error given by Eq. (48) is quantum-optimal in terms of its scaling with the object size.

It is noteworthy that the quantum bound is invariant to any unitary operation on the image-plane light, so the bound is applicable to more general indirect imaging systems, such as stellar interferometry, that are diffraction-limited but do not necessarily have a physical image plane in its setup.

## V. PRACTICAL CONCERNS AND OPEN PROBLEMS

It is important to note that the theory here assumes ideal conditions for both SPADE and direct imaging. For SPADE, perfect demultiplexing in the PAD basis and perfect interferometry are assumed, while for direct imaging, an infinitesimal pixel size, an infinite number of pixels with no gaps inbetween, and no interpixel crosstalk are assumed. For both methods, the object is assumed to have a strict subdiffraction size, and no excess noise other than photon shot noise are assumed in the photodetection.

A fair comparison of SPADE and direct imaging under practical conditions is difficult to perform in theory, as they involve very different optics and may be affected by current technical limitations in very different ways. Here I only highlight one practical concern for SPADE, which is crosstalk among the channels [61]. An intuitive reason for the superiority of SPADE is that the filtering of the lower-order modes from each channel reduces the output variance by reducing the expected photon count given by Eq. (39) while retaining some sensitivity to certain moments. If the  $q$ th output of the PAD-basis demultiplexer is contaminated by some lower-order modes, the transition amplitude given by Eq. (33) would contain lower-order monomials ( $\propto X^p$  with  $p < q$ ), which in

turn introduce lower-order moments to the expected photon count given by Eq. (39). The bias due to these parasitic terms may be corrected if the lower-order modes and therefore the lower-order moments are also measured. Of more fundamental concern is the increase in the variance that is also proportional to the expected photon count. This variance increase leads to a suboptimal error scaling with  $\Delta$  for small  $\Delta$ .

Direct imaging under current technology is, of course, not perfect either, and a useful comparison between the two methods under practical conditions is perhaps best performed with experiments.

On the theoretical side, the exact quantum optimality of the proposal here for the semiparametric problem remains an open question. On one hand, a more exact computation of the quantum bound than the one discussed in Sec. IV-C is needed and not at all trivial for the semiparametric problem because of the infinite dimensionality [10], [60]. On the other hand, it may be possible to optimize the scheme further by more complicated interferometry.

Another interesting open problem is density estimation: the reconstruction of the object intensity via the moments or the Fourier coefficients, taking into account the positivity of the intensity and any other prior information. More advanced statistical methods will be required to study the estimators, the performances, and the limits [62].

Finally, I should mention that the paraxial approximation and the assumption of incoherent light from the object are idealizations and may introduce systematic errors in practice. Given the small numerical aperture (N.A.) in astronomy and remote sensing, there is no reason to doubt the accuracy of the paraxial approximation there, but one may need the full electromagnetic field theory to accurately model high-N.A. microscopy [63], [64], [65]. As the concept of spatial modes remains valid in the full field theory [66], a generalization of SPADE for high-N.A. imaging would be complicated but possible.

There is also some recent academic interest in partially coherent sources [14], [67], [68], [69], [70]. The optical fields from any object must have a nonzero coherence length in principle [69], [71]. The coherence length of astronomical sources should be on the order of the wavelength [71], which is so much smaller than all the other length scales in the imaging problem that it is unlikely to make any noticeable difference in astronomy. Although partial coherence may be more important to sensing and microscopy, there is a dearth of experiments characterizing the coherence in those applications, making it difficult to even write down a realistic partially coherent model, let alone perform a useful analysis. Until a better model emerges, the incoherent model remains the gold standard in both astronomy [39], [42] and fluorescence microscopy [22].

## VI. CONCLUSION

I have proposed a superoscillation measurement scheme for incoherent imaging that overcomes the key limitations of previous superoscillation techniques, such as inefficiency and questionable advantage over computational techniques. Provably superior to direct imaging and close to the quantum

limit, the scheme put forth is efficient in terms of both photon collection and statistical performance. The theory shares similarities with several superresolution concepts, thus establishing a common foundation for future superresolution research.

To be sure, an implementation of SPADE with high efficiency and fidelity is not trivial in practice. Its fundamental superiority, the importance of the applications, and the rapid experimental progress in photonics [44], [46], [43], [72] should, nonetheless, offer encouragement for its further development.

## REFERENCES

- [1] G. de Villiers and E. R. Pike, *The Limits of Resolution*. Boca Raton: CRC Press, 2016. doi: [10.1201/9781315366708](https://doi.org/10.1201/9781315366708)
- [2] M. Berry, N. Zheludev, Y. Aharonov, F. Colombo, I. Sabadini, D. C. Struppa, J. Tollaksen, E. T. F. Rogers, F. Qin, M. Hong, X. Luo, R. Remez, A. Arie, J. B. Götte, M. R. Dennis, A. M. H. Wong, G. V. Eleftheriades, Y. Eliezer, A. Bahabad, G. Chen, Z. Wen, G. Liang, C. Hao, C.-W. Qiu, A. Kempf, E. Katzav, and M. Schwartz, “Roadmap on superoscillations,” *Journal of Optics*, vol. 21, no. 5, p. 053002, Apr. 2019. doi: [10.1088/2040-8986/ab0191](https://doi.org/10.1088/2040-8986/ab0191). [Online]. Available: <https://doi.org/10.1088%2F2040-8986%2Fab0191>
- [3] M. Tsang, R. Nair, and X.-M. Lu, “Quantum theory of superresolution for two incoherent optical point sources,” *Physical Review X*, vol. 6, p. 031033, Aug. 2016. doi: [10.1103/PhysRevX.6.031033](https://doi.org/10.1103/PhysRevX.6.031033). [Online]. Available: <http://link.aps.org/doi/10.1103/PhysRevX.6.031033>
- [4] M. Tsang, “Resolving starlight: a quantum perspective,” *Contemporary Physics*, vol. 60, no. 4, pp. 279–298, Oct. 2019. doi: [10.1080/00107514.2020.1736375](https://doi.org/10.1080/00107514.2020.1736375). [Online]. Available: <https://doi.org/10.1080/00107514.2020.1736375>
- [5] C. W. Helstrom, *Quantum Detection and Estimation Theory*. New York: Academic Press, 1976. [Online]. Available: <http://www.sciencedirect.com/science/bookseries/00765392/123>
- [6] M. Tsang, “Subdiffraction incoherent optical imaging via spatial-mode demultiplexing,” *New Journal of Physics*, vol. 19, no. 2, p. 023054, 2017. doi: [10.1088/1367-2630/aa60ee](https://doi.org/10.1088/1367-2630/aa60ee). [Online]. Available: <http://stacks.iop.org/1367-2630/19/i=2/a=023054>
- [7] —, “Subdiffraction incoherent optical imaging via spatial-mode demultiplexing: Semiclassical treatment,” *Physical Review A*, vol. 97, no. 2, p. 023830, Feb. 2018. doi: [10.1103/PhysRevA.97.023830](https://doi.org/10.1103/PhysRevA.97.023830). [Online]. Available: <https://link.aps.org/doi/10.1103/PhysRevA.97.023830>
- [8] —, “Quantum limit to subdiffraction incoherent optical imaging,” *Physical Review A*, vol. 99, no. 1, p. 012305, Jan. 2019. doi: [10.1103/PhysRevA.99.012305](https://doi.org/10.1103/PhysRevA.99.012305). [Online]. Available: <https://link.aps.org/doi/10.1103/PhysRevA.99.012305>
- [9] —, “Semiparametric estimation for incoherent optical imaging,” *Physical Review Research*, vol. 1, no. 3, p. 033006, Oct. 2019. doi: [10.1103/PhysRevResearch.1.033006](https://doi.org/10.1103/PhysRevResearch.1.033006). [Online]. Available: <https://link.aps.org/doi/10.1103/PhysRevResearch.1.033006>
- [10] —, “Quantum limit to subdiffraction incoherent optical imaging. II. A parametric-submodel approach,” *Physical Review A*, vol. 104, no. 5, p. 052411, Nov. 2021. doi: [10.1103/PhysRevA.104.052411](https://doi.org/10.1103/PhysRevA.104.052411). [Online]. Available: <https://link.aps.org/doi/10.1103/PhysRevA.104.052411>
- [11] F. Yang, A. Tashchilina, E. S. Moiseev, C. Simon, and A. I. Lvovsky, “Far-field linear optical superresolution via heterodyne detection in a higher-order local oscillator mode,” *Optica*, vol. 3, no. 10, p. 1148, Oct. 2016. doi: [10.1364/OPTICA.3.001148](https://doi.org/10.1364/OPTICA.3.001148). [Online]. Available: <https://www.osapublishing.org/abstract.cfm?URI=optica-3-10-1148>
- [12] S. Zhou and L. Jiang, “Modern description of Rayleigh’s criterion,” *Physical Review A*, vol. 99, no. 1, p. 013808, Jan. 2019. doi: [10.1103/PhysRevA.99.013808](https://doi.org/10.1103/PhysRevA.99.013808). [Online]. Available: <https://link.aps.org/doi/10.1103/PhysRevA.99.013808>
- [13] K. A. G. Bonsma-Fisher, W.-K. Tham, H. Ferretti, and A. M. Steinberg, “Realistic sub-Rayleigh imaging with phase-sensitive measurements,” *New Journal of Physics*, vol. 21, no. 9, p. 093010, Sep. 2019. doi: [10.1088/1367-2630/ab3d97](https://doi.org/10.1088/1367-2630/ab3d97). [Online]. Available: <https://doi.org/10.1088%2F1367-2630%2Fab3d97>
- [14] K. Liang, S. A. Wadood, and A. N. Vamivakas, “Coherence effects on estimating general sub-Rayleigh object distribution moments,” *Physical Review A*, vol. 104, no. 2, p. 022220, Aug. 2021. doi: [10.1103/PhysRevA.104.022220](https://doi.org/10.1103/PhysRevA.104.022220). [Online]. Available: <https://link.aps.org/doi/10.1103/PhysRevA.104.022220>
- [15] D. Slepian, “Some Comments on Fourier Analysis, Uncertainty and Modeling,” *SIAM Review*, vol. 25, no. 3, pp. 379–393, 1983. [Online]. Available: <https://www.jstor.org/stable/2029386>
- [16] M. Bertero and C. de Mol, “III Super-Resolution by Data Inversion,” in *Progress in Optics*, E. Wolf, Ed. Amsterdam: Elsevier, 1996, vol. 36, pp. 129–178. [Online]. Available: <http://www.sciencedirect.com/science/article/pii/S0079663808703147>
- [17] J. G. Walker, G. J. Brakenhoff, M. Bertero, E. R. Pike, R. E. Davies, and M. R. Young, “Superresolving scanning optical microscopy using holographic optical processing,” *Journal of the Optical Society of America A*, vol. 10, no. 1, pp. 59–64, Jan. 1993. doi: [10.1364/JOSAA.10.000059](https://doi.org/10.1364/JOSAA.10.000059). [Online]. Available: <http://www.osapublishing.org/abstract.cfm?uri=josaa-10-1-59>
- [18] M. I. Kolobov and C. Fabre, “Quantum limits on optical resolution,” *Physical Review Letters*, vol. 85, pp. 3789–3792, Oct. 2000. doi: [10.1103/PhysRevLett.85.3789](https://doi.org/10.1103/PhysRevLett.85.3789). [Online]. Available: <http://link.aps.org/doi/10.1103/PhysRevLett.85.3789>
- [19] V. N. Beskrovnyy and M. I. Kolobov, “Quantum limits of super-resolution in reconstruction of optical objects,” *Physical Review A*, vol. 71, p. 043802, Apr. 2005. doi: [10.1103/PhysRevA.71.043802](https://doi.org/10.1103/PhysRevA.71.043802). [Online]. Available: <http://link.aps.org/doi/10.1103/PhysRevA.71.043802>
- [20] V. N. Beskrovnyy and M. I. Kolobov, “Quantum-statistical analysis of superresolution for optical systems with circular symmetry,” *Physical Review A*, vol. 78, p. 043824, Oct. 2008. doi: [10.1103/PhysRevA.78.043824](https://doi.org/10.1103/PhysRevA.78.043824). [Online]. Available: <http://link.aps.org/doi/10.1103/PhysRevA.78.043824>
- [21] K. Piché, J. Leach, A. S. Johnson, J. Z. Salvail, M. I. Kolobov, and R. W. Boyd, “Experimental realization of optical eigenmode super-resolution,” *Opt. Express*, vol. 20, no. 24, pp. 26424–26433, Nov. 2012. doi: [10.1364/OE.20.026424](https://doi.org/10.1364/OE.20.026424). [Online]. Available: <http://www.opticsexpress.org/abstract.cfm?URI=oe-20-24-26424>
- [22] J. B. Pawley, Ed., *Handbook of Biological Confocal Microscopy*. New York: Springer, 2006. doi: [10.1007/978-0-387-45524-2](https://doi.org/10.1007/978-0-387-45524-2)
- [23] W. E. Moerner, “Nobel Lecture: Single-molecule spectroscopy, imaging, and photocontrol: Foundations for super-resolution microscopy,” *Reviews of Modern Physics*, vol. 87, no. 4, pp. 1183–1212, Oct. 2015. doi: [10.1103/RevModPhys.87.1183](https://doi.org/10.1103/RevModPhys.87.1183). [Online]. Available: <https://link.aps.org/doi/10.1103/RevModPhys.87.1183>
- [24] E. Betzig, “Nobel Lecture: Single molecules, cells, and super-resolution optics,” *Reviews of Modern Physics*, vol. 87, no. 4, pp. 1153–1168, Oct. 2015. doi: [10.1103/RevModPhys.87.1153](https://doi.org/10.1103/RevModPhys.87.1153). [Online]. Available: <https://link.aps.org/doi/10.1103/RevModPhys.87.1153>
- [25] S. W. Hell, “Nobel Lecture: Nanoscopy with freely propagating light,” *Reviews of Modern Physics*, vol. 87, no. 4, pp. 1169–1181, Oct. 2015. doi: [10.1103/RevModPhys.87.1169](https://doi.org/10.1103/RevModPhys.87.1169). [Online]. Available: <https://link.aps.org/doi/10.1103/RevModPhys.87.1169>
- [26] J. W. Goodman, *Introduction to Fourier Optics*. New York: McGraw-Hill, 2004.
- [27] G. Schiebinger, E. Robeva, and B. Recht, “Superresolution without separation,” *Information and Inference: A Journal of the IMA*, vol. 7, pp. 1–30, 2018. doi: [10.1093/imaia/iax006](https://doi.org/10.1093/imaia/iax006)
- [28] E. Bisketzi, D. Branford, and A. Datta, “Quantum limits of localisation microscopy,” *New Journal of Physics*, vol. 21, no. 12, p. 123032, Dec. 2019. doi: [10.1088/1367-2630/ab58a0](https://doi.org/10.1088/1367-2630/ab58a0). [Online]. Available: <https://doi.org/10.1088%2F1367-2630%2Fab58a0>
- [29] Z. Dutton, R. Kerviche, A. Ashok, and S. Guha, “Attaining the quantum limit of superresolution in imaging an object’s length via predetection spatial-mode sorting,” *Physical Review A*, vol. 99, no. 3, p. 033847, Mar. 2019. doi: [10.1103/PhysRevA.99.033847](https://doi.org/10.1103/PhysRevA.99.033847). [Online]. Available: <https://link.aps.org/doi/10.1103/PhysRevA.99.033847>
- [30] H. Krovi, “Superresolution at the quantum limit beyond two point sources,” *arXiv:2206.14788 [physics, physics:quant-ph]*, Jun. 2022. doi: [10.48550/arXiv.2206.14788](https://doi.org/10.48550/arXiv.2206.14788). [Online]. Available: <http://arxiv.org/abs/2206.14788>
- [31] P. J. Bickel, C. A. J. Klaassen, Y. Ritov, and J. A. Wellner, *Efficient and Adaptive Estimation for Semiparametric Models*. New York: Springer, 1993.
- [32] K. K. M. Bearne, K. K. M. Bearne, Y. Zhou, Y. Zhou, B. Braverman, J. Yang, S. A. Wadood, A. N. Jordan, A. N. Jordan, A. N. Vamivakas, A. N. Vamivakas, A. N. Vamivakas, Z. Shi, R. W. Boyd, R. W. Boyd, and R. W. Boyd, “Confocal super-resolution microscopy based on a spatial mode sorter,” *Optics Express*, vol. 29, no. 8, pp. 11784–11792, Apr. 2021. doi: [10.1364/OE.419493](https://doi.org/10.1364/OE.419493). [Online]. Available: <https://www.osapublishing.org/oe/abstract.cfm?uri=oe-29-8-11784>
- [33] E. F. Matlin and L. J. Zipp, “Imaging arbitrary incoherent source distributions with near quantum-limited resolution,” *Scientific Reports*, vol. 12, no. 1, p. 2810, Feb. 2022. doi: [10.1038/s41598-022-02810-1](https://doi.org/10.1038/s41598-022-02810-1)



- 022-06644-3. [Online]. Available: <https://www.nature.com/articles/s41598-022-06644-3>
- [34] G. Toraldo di Francia, "Super-gain antennas and optical resolving power," *Il Nuovo Cimento (1943-1954)*, vol. 9, no. 3, pp. 426–438, Mar. 1952. doi: [10.1007/BF02903413](https://doi.org/10.1007/BF02903413). [Online]. Available: <https://doi.org/10.1007/BF02903413>
- [35] F. M. Huang and N. I. Zheludev, "Super-resolution without evanescent waves," *Nano Letters*, vol. 9, no. 3, pp. 1249–1254, 2009. doi: [10.1021/nl9002014](https://doi.org/10.1021/nl9002014). [Online]. Available: <http://dx.doi.org/10.1021/nl9002014>
- [36] C. J. R. Sheppard, "Super-resolution in confocal imaging," *Optik*, vol. 80, p. 53, 1988.
- [37] C. B. Müller and J. Enderlein, "Image Scanning Microscopy," *Physical Review Letters*, vol. 104, no. 19, p. 198101, May 2010. doi: [10.1103/PhysRevLett.104.198101](https://doi.org/10.1103/PhysRevLett.104.198101). [Online]. Available: <https://link.aps.org/doi/10.1103/PhysRevLett.104.198101>
- [38] F. W. J. Olver, D. W. Lozier, R. F. Boisvert, and C. W. Clark, Eds., *NIST Handbook of Mathematical Functions*. Cambridge: NIST and Cambridge University Press, 2010.
- [39] J. W. Goodman, *Statistical Optics*. New York: Wiley, 1985.
- [40] J. Řeháček, M. Paúr, B. Stoklasa, Z. Hradil, and L. L. Sánchez-Soto, "Optimal measurements for resolution beyond the Rayleigh limit," *Optics Letters*, vol. 42, no. 2, pp. 231–234, Jan. 2017. doi: [10.1364/OL.42.000231](https://doi.org/10.1364/OL.42.000231). [Online]. Available: <http://www.osapublishing.org/abstract.cfm?uri=ol-42-2-231>
- [41] K. R. Parthasarathy, *Introduction to Probability and Measure*. New Delhi: Hindustan Book Agency, 2005. ISBN 9789386279279. doi: [10.1007/978-93-86279-27-9](https://doi.org/10.1007/978-93-86279-27-9). [Online]. Available: <https://www.springer.com/gp/book/9789386279279>
- [42] J. Zmuidzinas, "Cramér–Rao sensitivity limits for astronomical instruments: implications for interferometer design," *Journal of the Optical Society of America A*, vol. 20, no. 2, pp. 218–233, Feb 2003. doi: [10.1364/JOSAA.20.000218](https://doi.org/10.1364/JOSAA.20.000218). [Online]. Available: <http://josaa.osa.org/abstract.cfm?URI=josaa-20-2-218>
- [43] M. Piccardo, V. Ginis, A. Forbes, S. Mahler, A. A. Friesem, N. Davidson, H. Ren, A. H. Dorrah, F. Capasso, F. T. Dullo, B. S. Ahluwalia, A. Ambrosio, S. Gigan, N. Treps, M. Hiekkamäki, R. Fickler, M. Kues, D. Moss, R. Morandotti, J. Riemensberger, T. J. Kippenberg, J. Faist, G. Scalari, N. Picqué, T. W. Hänsch, G. Cerullo, C. Manzoni, L. A. Lugiato, M. Brambilla, L. Columbo, A. Gatti, F. Prati, A. Shiri, A. F. Abouraddy, A. Alù, E. Galiffi, J. B. Pendry, and P. A. Huidobro, "Roadmap on multimode light shaping," *Journal of Optics*, vol. 24, no. 1, p. 013001, Dec. 2021. doi: [10.1088/2040-8986/ac3a9d](https://doi.org/10.1088/2040-8986/ac3a9d). [Online]. Available: <https://doi.org/10.1088/2040-8986/ac3a9d>
- [44] P. Boucher, C. Fabre, G. Labroille, and N. Treps, "Spatial optical mode demultiplexing as a practical tool for optimal transverse distance estimation," *Optica*, vol. 7, no. 11, pp. 1621–1626, Nov 2020. doi: [10.1364/OPTICA.404746](https://doi.org/10.1364/OPTICA.404746). [Online]. Available: <http://www.osapublishing.org/optica/abstract.cfm?URI=optica-7-11-1621>
- [45] J.-F. Morizur, L. Nicholls, P. Jian, S. Armstrong, N. Treps, B. Hage, M. Hsu, W. Bowen, J. Janousek, and H.-A. Bachor, "Programmable unitary spatial mode manipulation," *Journal of the Optical Society of America A*, vol. 27, no. 11, pp. 2524–2531, Nov 2010. doi: [10.1364/JOSAA.27.002524](https://doi.org/10.1364/JOSAA.27.002524). [Online]. Available: <http://josaa.osa.org/abstract.cfm?URI=josaa-27-11-2524>
- [46] N. K. Fontaine, R. Ryf, H. Chen, D. T. Neilson, K. Kim, and J. Carpenter, "Laguerre-Gaussian mode sorter," *Nature Communications*, vol. 10, no. 1, p. 1865, Apr. 2019. doi: [10.1038/s41467-019-09840-4](https://doi.org/10.1038/s41467-019-09840-4). [Online]. Available: <http://www.nature.com/articles/s41467-019-09840-4>
- [47] W.-K. Tham, H. Ferretti, and A. M. Steinberg, "Beating Rayleigh's Curse by Imaging Using Phase Information," *Physical Review Letters*, vol. 118, no. 7, p. 070801, Feb. 2017. doi: [10.1103/PhysRevLett.118.070801](https://doi.org/10.1103/PhysRevLett.118.070801). [Online]. Available: <https://link.aps.org/doi/10.1103/PhysRevLett.118.070801>
- [48] J. M. Donohue, V. Ansari, J. Řeháček, Z. Hradil, B. Stoklasa, M. Paúr, L. L. Sánchez-Soto, and C. Silberhorn, "Quantum-Limited Time-Frequency Estimation through Mode-Selective Photon Measurement," *Physical Review Letters*, vol. 121, no. 9, p. 090501, Aug. 2018. doi: [10.1103/PhysRevLett.121.090501](https://doi.org/10.1103/PhysRevLett.121.090501). [Online]. Available: <https://link.aps.org/doi/10.1103/PhysRevLett.121.090501>
- [49] H. Zhang, H. Zhang, S. Kumar, S. Kumar, Y.-P. Huang, and Y.-P. Huang, "Super-resolution optical classifier with high photon efficiency," *Optics Letters*, vol. 45, no. 18, pp. 4968–4971, Sep. 2020. doi: [10.1364/OL.401614](https://doi.org/10.1364/OL.401614). [Online]. Available: <https://opg.optica.org/ol/abstract.cfm?uri=ol-45-18-4968>
- [50] V. Ansari, B. Brecht, J. Gil-Lopez, J. M. Donohue, J. Řeháček, Z. Hradil, L. L. Sánchez-Soto, and C. Silberhorn, "Achieving the Ultimate Quantum Timing Resolution," *PRX Quantum*, vol. 2, no. 1, p. 010301, Jan. 2021. doi: [10.1103/PRXQuantum.2.010301](https://doi.org/10.1103/PRXQuantum.2.010301). [Online]. Available: <https://link.aps.org/doi/10.1103/PRXQuantum.2.010301>
- [51] R. Nair and M. Tsang, "Interferometric superlocalization of two incoherent optical point sources," *Optics Express*, vol. 24, no. 4, pp. 3684–3701, Feb 2016. doi: [10.1364/OE.24.003684](https://doi.org/10.1364/OE.24.003684). [Online]. Available: <http://www.opticsexpress.org/abstract.cfm?URI=oe-24-4-3684>
- [52] Z. S. Tang, K. Durak, and A. Ling, "Fault-tolerant and finite-error localization for point emitters within the diffraction limit," *Optics Express*, vol. 24, no. 19, p. 22004, Sep. 2016. doi: [10.1364/OE.24.022004](https://doi.org/10.1364/OE.24.022004). [Online]. Available: <https://www.osapublishing.org/abstract.cfm?URI=oe-24-19-22004>
- [53] A. A. Pushkina, G. Maltese, J. I. Costa-Filho, P. Patel, and A. I. Lvovsky, "Superresolution Linear Optical Imaging in the Far Field," *Physical Review Letters*, vol. 127, no. 25, p. 253602, Dec. 2021. doi: [10.1103/PhysRevLett.127.253602](https://doi.org/10.1103/PhysRevLett.127.253602). [Online]. Available: <https://link.aps.org/doi/10.1103/PhysRevLett.127.253602>
- [54] O. Guyon, E. A. Pluzhnik, M. J. Kuchner, B. Collins, and S. T. Ridgway, "Theoretical limits on extrasolar terrestrial planet detection with coronagraphs," *The Astrophysical Journal Supplement Series*, vol. 167, pp. 81–99, 2006. doi: [10.1086/507630](https://doi.org/10.1086/507630)
- [55] E. Serabyn, B. Mennesson, S. Martin, K. Liewer, and J. Kühn, "Nulling at short wavelengths: theoretical performance constraints and a demonstration of faint companion detection inside the diffraction limit with a rotating-baseline interferometer," *Monthly Notices of the Royal Astronomical Society*, vol. 489, no. 1, pp. 1291–1303, 08 2019. doi: [10.1093/mnras/stz2163](https://doi.org/10.1093/mnras/stz2163). [Online]. Available: <https://doi.org/10.1093/mnras/stz2163>
- [56] A. Labeyrie, S. G. Lipson, and P. Nisenson, *An Introduction to Optical Stellar Interferometry*. Cambridge: Cambridge University Press, 2006. ISBN 9780511617638. doi: [10.1017/CBO9780511617638](https://doi.org/10.1017/CBO9780511617638). [Online]. Available: <http://dx.doi.org/10.1017/CBO9780511617638>
- [57] M. Mazelanik, A. Leszczyński, and M. Parniak, "Optical-domain spectral super-resolution via a quantum-memory-based time-frequency processor," *Nature Communications*, vol. 13, no. 1, p. 691, Feb. 2022. doi: [10.1038/s41467-022-28066-5](https://doi.org/10.1038/s41467-022-28066-5). [Online]. Available: <https://www.nature.com/articles/s41467-022-28066-5>
- [58] D. E. Knuth, "Big Omicron and big Omega and big Theta," *ACM SIGACT News*, vol. 8, no. 2, pp. 18–24, Apr. 1976. doi: [10.1145/1008328.1008329](https://doi.org/10.1145/1008328.1008329). [Online]. Available: <https://doi.org/10.1145/1008328.1008329>
- [59] M. Paúr, B. Stoklasa, J. Grover, A. Krzic, L. L. Sánchez-Soto, Z. Hradil, and J. Řeháček, "Tempering Rayleigh's curse with PSF shaping," *Optica*, vol. 5, no. 10, pp. 1177–1180, Oct. 2018. doi: [10.1364/OPTICA.5.001177](https://doi.org/10.1364/OPTICA.5.001177). [Online]. Available: <http://www.osapublishing.org/optica/abstract.cfm?uri=optica-5-10-1177>
- [60] M. Tsang, F. Albarelli, and A. Datta, "Quantum Semiparametric Estimation," *Physical Review X*, vol. 10, no. 3, p. 031023, Jul. 2020. doi: [10.1103/PhysRevX.10.031023](https://doi.org/10.1103/PhysRevX.10.031023). [Online]. Available: <https://link.aps.org/doi/10.1103/PhysRevX.10.031023>
- [61] M. Gessner, C. Fabre, and N. Treps, "Superresolution Limits from Measurement Crosstalk," *Physical Review Letters*, vol. 125, no. 10, p. 100501, Aug. 2020. doi: [10.1103/PhysRevLett.125.100501](https://doi.org/10.1103/PhysRevLett.125.100501). [Online]. Available: <https://link.aps.org/doi/10.1103/PhysRevLett.125.100501>
- [62] A. B. Tsybakov, *Introduction to Nonparametric Estimation*. New York: Springer, 2009. doi: [10.1007/b13794](https://doi.org/10.1007/b13794)
- [63] K. I. Mortensen, L. S. Churchman, J. A. Spudich, and H. Flyvbjerg, "Optimized localization analysis for single-molecule tracking and super-resolution microscopy," *Nature Methods*, vol. 7, no. 5, pp. 377–381, May 2010. doi: [10.1038/nmeth.1447](https://doi.org/10.1038/nmeth.1447). [Online]. Available: <http://www.nature.com/nmeth/journal/v7/n5/abs/nmeth.1447.html>
- [64] M. Tsang, "Quantum limits to optical point-source localization," *Optica*, vol. 2, no. 7, pp. 646–653, Jul 2015. doi: [10.1364/OPTICA.2.000646](https://doi.org/10.1364/OPTICA.2.000646). [Online]. Available: <http://www.osapublishing.org/optica/abstract.cfm?URI=optica-2-7-646>
- [65] O. Zhang and M. D. Lew, "Single-molecule orientation localization microscopy i: fundamental limits," *J. Opt. Soc. Am. A*, vol. 38, no. 2, pp. 277–287, Feb 2021. doi: [10.1364/JOSAA.411981](https://doi.org/10.1364/JOSAA.411981). [Online]. Available: <http://opg.optica.org/josaa/abstract.cfm?URI=josaa-38-2-277>
- [66] C. Fabre and N. Treps, "Modes and states in quantum optics," *Reviews of Modern Physics*, vol. 92, no. 3, p. 035005, Sep. 2020. doi: [10.1103/RevModPhys.92.035005](https://doi.org/10.1103/RevModPhys.92.035005). [Online]. Available: <https://link.aps.org/doi/10.1103/RevModPhys.92.035005>
- [67] W. Larson and B. E. A. Saleh, "Resurgence of Rayleigh's curse in the presence of partial coherence," *Optica*, vol. 5, no. 11, pp. 1382–1389, Nov. 2018. doi: [10.1364/OPTICA.5.001382](https://doi.org/10.1364/OPTICA.5.001382). [Online]. Available: <http://www.osapublishing.org/optica/abstract.cfm?uri=optica-5-11-1382>



- [68] Z. Hradil, D. Koutný, and J. Řeháček, “Exploring the ultimate limits: super-resolution enhanced by partial coherence,” *Optics Letters*, vol. 46, no. 7, pp. 1728–1731, Apr. 2021. doi: [10.1364/OL.417988](https://doi.org/10.1364/OL.417988). [Online]. Available: <https://www.osapublishing.org/ol/abstract.cfm?uri=ol-46-7-1728>
- [69] S. Kurdzialek, “Back to sources – the role of losses and coherence in super-resolution imaging revisited,” *Quantum*, vol. 6, p. 697, Apr. 2022. doi: [10.22331/q-2022-04-27-697](https://doi.org/10.22331/q-2022-04-27-697). [Online]. Available: <https://quantum-journal.org/papers/q-2022-04-27-697/>
- [70] M. Tsang, “Poisson Quantum Information,” *Quantum*, vol. 5, p. 527, Aug. 2021. doi: [10.22331/q-2021-08-19-527](https://doi.org/10.22331/q-2021-08-19-527). [Online]. Available: <https://quantum-journal.org/papers/q-2021-08-19-527/>
- [71] M. Born and E. Wolf, *Principles of Optics*. Cambridge: Cambridge University Press, 2019. doi: [10.1017/9781108769914](https://doi.org/10.1017/9781108769914)
- [72] B. Norris and J. Bland-Hawthorn, “Astrophotonics: the rise of integrated photonics in astronomy,” *Optics and Photonics News*, vol. 30(5), pp. 26–33, May 2019. doi: [10.1364/OPN.30.5.000026](https://doi.org/10.1364/OPN.30.5.000026)